3D CT to 2D Low Dose Single-Plane Fluoroscopy Registration Algorithm for In-vivo Knee Motion Analysis

Masuma Akter[1*], Andrew J. Lambert[1], Mark R. Pickering[1], Jennie M. Scarvell[2] and Paul N. Smith[2]
[1]*School of Engineering and Information Technology, University of New South Wales, Canberra, Australia.*;
[2] *Department of Surgery, The Canberra Hospital, Canberra, Australia*

***Abstract*— A limitation to accurate automatic tracking of knee motion is the noise and blurring present in low dose X-ray fluoroscopy images. For more accurate tracking, this noise should be reduced while preserving anatomical structures such as bone. Noise in low dose X-ray images is generated from different sources, however quantum noise is by far the most dominant. In this paper we present an accurate multi-modal image registration algorithm which successfully registers 3D CT to 2D single plane low dose noisy and blurred fluoroscopy images that are captured for healthy knees. The proposed algorithm uses a new registration framework including a filtering method to reduce the noise and blurring effect in fluoroscopy images. Our experimental results show that the extra pre-filtering step included in the proposed approach maintains higher accuracy and repeatability for in vivo knee joint motion analysis.**

***Index Terms*— 3D-2D Registration, kinematic analysis, quantum noise, blind deconvolution, Wiener filter.**

I. INTRODUCTION

Fluoroscopy captures real-time X-ray images that are helpful for guiding a surgeon for diagnostic and interventional processes. These processes include total knee arthroplasty (TKA), and treatment for knee ligament rupture and injuries. However, the high ionizing radiation exposure is a significant factor in the image capturing process. Less X-ray exposure is required to take a fluoroscopic image, however harmful effects to the patient are possible during video fluoroscopy due to a longer period of X-ray exposure in a particular part of the body. This total radiation dose to the patient during the capture process is significant and X-ray radiation should be reduced if possible for a safer image capture process. Hence, the fluoroscopy video is captured during dynamic motion with very low dose X-ray radiation to avoid radiation related injuries. The number of X-ray quanta per pixel reported in various studies is about 35 on average [1], [2]. This low dose X-ray leads to considerable degradation in image quality through quantum noise due to an irregular number of quanta arriving at the image intensifier. The captured images also contain non-linear noise, pincushion distortion due to the curved nature of the image intensifier and blurring effects for a moving subject.

A number of studies on reducing noise in low dose X-ray images have been reported. The most simple method is the use of a linear filter composed of temporal or spatial low pass filters. Although this filtering helps to reduce noise, this process also reduces image information such as edges. Thus, these filters are not suitable for object localization based on edge detection or cross correlation methods [3]. More complex digital processing methods and denoising approaches can be employed to overcome the limitations of linear filters. A number of different filters have been developed for this purpose including: edge-preserving adaptive filters [3], [4], adaptive variational denoising [5], non local-means filtering [6], image denoising based on wavelet-domain hidden Markov models [7], sparse and redundant representations over learned dictionaries [8], total least squares approaches [9] or partial differential equation techniques [10]. These filtering approaches provide a better trade-off between the amount of noise reduction and edge-preservation. However no studies have been reported for the removal of the motion blurring effect along with signal-dependent noise in fluoroscopy images. In this work, both of these image degradation effects are considered simultaneously.

There are a number of requirements to be considered for any registration algorithm in medical applications for in-vivo joint kinematics. These requirements include high accuracy, low computational cost, non-invasiveness, invariance to motion blur in the dynamic image, less operator interaction with the algorithm. For clinical applications such as diagnoses of pathologies, pre-operative planning and post-operative monitoring of patients, higher accuracy for low-dose radiography and non-invasiveness are the highest priority requirements for the algorithm.

The contribution of this paper is to demonstrate a new non-invasive 3D-2D registration framework which achieves improved accuracy when using noisy fluoroscopy data of dynamic movements acquired using a low dose of X-ray exposure. A 3D-2D registration framework using CT to single-plane fluoroscopy [11], [12], [13] is used to show the effectiveness of the proposed approach. The proposed registration approach contains two novel components 1) a new filter implementation which reduces the effect of noise and motion blurring using blind deconvolution and Wiener filtering in the spectral domain 2) A hybrid optimization approach which allows accurate measurement of out-of-plane translation and rotation motions using cross correlation (CC) in the frequency domain. To evaluate the performance of this algorithm, repeatability experiments were conducted using several in-vivo data sets where the subjects are performing

*Corresponding author. Email: masuma01@gmail.com

978-1-4244-7929-0/14/$26.00

a deep knee bend activity.

II. Proposed 3D-2D Registration Algorithm

Herein the 3D rigid body transform parameters correspond to directions in the the CT anatomical coordinate system as follows. Translations are expressed in the T_x (anterior-posterior), T_y (proximal-distal) and T_z (medial-lateral) directions and rotation about the X, Y, and Z axis correspond to R_x (abduction/adduction), R_y (internal/external rotation) and R_z (flexion/extension) respectively. The XY plane is considered to be the image plane and the Z axis is the X-ray beam projection direction.

The general flow of the proposed 3D-2D registration process is shown in Fig. 1. The real fluoroscopy image suffers from pincushion distortion caused by the curved shape of the image intensifier. This distortion is corrected using a 5th order polynomial function. Additionally, the fluoroscopy images contain quantum noise and a motion blurring effect explained in detail at the end of this section. These image degradation effects are reduced by using a deconvolution method in two steps. At first, a blind deconvolution method is used to estimate the point spread function (PSF) and the restored image corresponding to the PSF. Then the PSF and partially restored fluoroscopy image are used as input to a Wiener filtering stage.

The original CT images contain the bone and soft tissue together. Segmentation is required to remove the soft tissue from the images. The segmentation of the CT is performed in a slice-by-slice way i.e. the soft tissue is removed manually from each slice of the CT image. The spatial resolution of the CT image is also different to that of the fluoroscopy, thus resampling is also performed using the cubic interpolation method before employing the registration process.

After generating the digitally reconstructed radiography (DRR) from the segmented CT image, the images are thresholded to remove noise and highlight the most dominant edges and then filtered using a newly designed LoG filter with a non-linear exponent denoted by n-LoG in a multi-resolution framework (three stages). Before employing the n-LoG filter, the DRR image is filtered using a circular average filter with radius of 0.5 pixels to smooth the image and to fill any empty pixels resulting from the interpolation process. The fluoroscopy image is also filtered with a circular averaging filter with radius of 2.50 pixels to remove the high frequency noise in the images. By this circular filtering process, both images (DRR and fluoroscopy) have similar frequency content and similar edges are produced for the optimization procedure and for the similarity measure. The new n-LoG filter is employed to enhance the image edges obtained using the conventional LoG filtering process.

In the next stage, estimates of R_x and R_y are found using cross correlation (CC) in the frequency domain. The final stage of the algorithm uses the gradient descent (GD) approach from [13] to fine-tune the four parameters $(T_x,\ T_y,\ T_z,\ R_z)$ simultaneously.

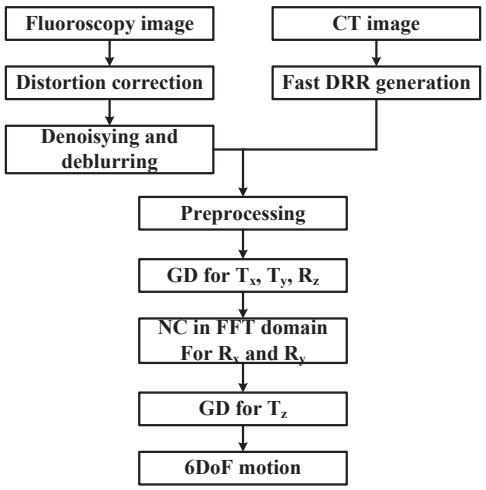

Fig. 1. The general flowchart of the proposed registration framework

A. Fluorosocopy noise modeling and filtering

Since X-ray radiation and attenuation in the bone and tissue are random processes, quantum or poisson noise is generated due to quantum fluctuation at the X-ray detector. This is not the only source of noise in the fluoroscopic image. Other noise sources are considered including scattered radiation and system noise, hardware noise (such as thermal, shot and quantisation noise). Due to this noise, the number of quanta incident on the detector in the exposure time, t_δ is not the same. However, quantum noise is the most dominating noise source, thus other noise can be neglected [2]. An example of quantum noise affected and blurred images are shown in Fig. 2.

1) Poisson Noise: A Poisson noise model can be formulated for X-ray images. The model parameters are linked to physical quantities and detector constants during the image acquisition process. For this model, it is assumed that the detected number N_d of X-ray quanta follow a Poisson distribution. Hence, the probability of N_d detected photons in an exposure time interval t_δ is

$$P_\lambda(X = N_d) = \frac{\lambda^{N_d}}{N_d!} e^{-\lambda_{N_d}} \tag{1}$$

$$\lambda = E[N_d] = \mu(N_d) = I_s/d_g \tag{2}$$

where the noise free photon count is λ when $d_o = 0$, the uncorrupted signal is I_s and the detector mapping is $I_r = d_g N_d + d_o$. E[] is the expected value of the noise N_d. In an image intensifier, the detected number of photons N_d is converted into an image pixel. In practice, the resulting raw image I_r is modelled as linearly dependent on the number of photons, i.e., with constant detector gain $d_g \in \mathbb{R}^+$ and offset $d_o \in \mathbb{R}^+$.

2) Gaussian Approximation: The Poisson model is not practically feasible for noise reduction methods. Thus, the quantum noise in low-dose X-ray images is approximated by zero-mean Gaussian noise with signal-dependent variance.

(a)

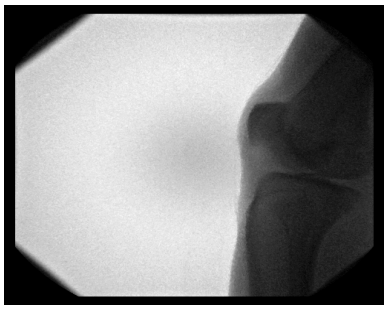

(b)

Fig. 2. An example of quantum noise and the effect of motion blurring in the fluoroscopy image during the image capturing process. (a) Blurred image. (b) Noisy image.

For large $\lambda >> 1$ the Poisson distribution of a discrete random variable X can be approximated by the sampled probability density function of a Gaussian distribution with the same mean and variance $\mu = \sigma^2 = \lambda$. The approximation improves with increasing λ.

3) Filter Process: The Wiener filter is given by

$$G(u,v) = \frac{1}{H(u,v)} \frac{|H(u,v)|^2}{|H(u,v)|^2 + S_n(u,v)/S_I(u,v)} \quad (3)$$

where $S_I(u,v)$ and $S_n(u,v)$ are the signal and noise power spectra respectively. $H(u,v)$ is the point spread function (PSF) that is generated using a blind deconvolution method. $S_I(u,v)$ is the restored fluoroscopy image from the blind deconvolution method. If the variance at each pixel is $\sigma_u^2 = 10^{PSNR/20}$, then the noise power spectrum is given as in (4) for an MxN image. This noise variance may be known using knowledge of the image acquisition process or may be estimated from the local variance of a smooth region of the image.

$$S_u(k,l) = MN\sigma_u^2 \quad (4)$$

III. Experimental Evaluation

A. Experimental data

For the dataset used in the experiments, healthy subjects were asked to freely move their knee to maximum bending position and back to the initial position to complete one cycle. Three sets of in-vivo data (specimen-A, specimen-B and specimen-C) for the dynamic deep knee bend activity of a healthy knee joint were used in the experiment. The image capture specifications for the raw data are shown in Table I. In this study, the in-vivo healthy knee images were taken using a curved panel detector at The Canberra Hospital, Australia.

TABLE I
Data set Specification of CT and X-ray images

	CT image	X-ray image
Manufacturer	Toshiba	Siemens
model	Aquilion	AXIOM-Artis
specimen-A	$512 \times 512 \times 452$ $0.445 \times 0.445 \times 0.5\ mm^3$	1024×1024 $0.244 \times 0.244\ mm^2$
specimen-B	$512 \times 512 \times 175$ $0.625 \times 0.625 \times 0.5\ mm^3$	512×512 $0.682 \times 0.682\ mm^2$
specimen-C	$512 \times 512 \times 496$ $0.520 \times 0.520 \times 0.5\ mm^3$	512×512 $0.682 \times 0.682\ mm^2$
digit	$16\ bits/pixel$	$12\ bits/pixel$

B. Evaluation scheme

To determine the effectiveness of the designed filtering method, filtered and raw fluoroscopy images were employed in the proposed registration framework explained in section-II. The images used in this experiment were of in-vivo healthy knees and no beads/markers were implanted, thus it is not possible to employ a standard ground truth for accuracy measurement. Recently, an automatic 3D-2D image matching method was developed and validated for its application to investigate human knee joint kinematics using fluoroscopic images [11]. In their study, repeatability measurements were used to estimate the performance of the registration framework [12]. Hence, in this study, we adopt a similar approach to determine the repeatability of the registration algorithm for the dynamic knee flexion motion in three healthy specimens (5 flexion positions). The 3D-2D registration framework measured repeatability over 20 optimisations per pose. The registration algorithm was performed individually for femur and tibia.

C. Results and discussion

1) Registration Results: Table II shows the average errors for three sets of sample images of femur and tibia bones (5 flexion positions from each samples) of specimen-A, specimen-B, and specimen-C. The maximum registration error expressed as $mean \pm repeatability$ for the case of out-of-plane translation for the femur and tibia was -0.13 ± 1.08 mm and -0.23 ± 1.09 mm respectively, when the proposed filter was employed on the noisy fluoroscopy images. Whereas, the accuracy of the same sample without employing the filter was -0.80 ± 3.14 mm and -5.2 ± 6.11

TABLE II

MEAN±REPEATABILITY OF THE REGISTRATION ERRORS FOR FILTERED IMAGES AND NON-FILTERED IMAGES AS THE AVERAGE ERRORS FOR FIVE FLUOROSCOPY IMAGES OF THE FEMUR AND THE TIBIA BONES OF SPECIMEN-A, SPECIMEN-B, AND SPECIMEN-C. THE TRANSLATION AND ROTATIONS ARE MEASURED IN (mm) AND $(^\circ)$ RESPECTIVELY.

sample	filter	bone	T_x	T_y	T_z	R_x	R_y	R_z
specimen-A	yes	femur	0.57±0.11	-0.03±0.50	0.20±1.06	-0.06±0.32	0.01±0.27	-0.19±0.13
		tibia	-0.61±0.27	0.04±0.01	-0.18±1.07	0.80±0.79	0.38±0.14	0.14±0.50
	no	femur	-0.89±0.19	0.83±0.70	-0.07±3.12	0.03±3.34	-0.05±3.06	-0.01±0.11
		tibia	-1.48±1.69	1.77±2.21	1.18±3.77	0.20±2.48	0.04±1.16	-0.67±1.27
specimen-B	yes	femur	0.58±0.12	-0.81±0.10	0.18±1.06	-0.18±0.69	0.24±0.53	-0.11±0.23
		tibia	-0.78±0.18	0.79±0.21	-0.14±1.08	0.35±0.51	0.38±0.20	-0.20±0.28
	no	femur	-1.20±0.19	2.21±0.70	1.58±3.13	-4.91±1.34	-4.85±1.30	1.64±0.33
		tibia	-0.13±0.33	-1.7±0.41	0.20±3.12	-0.04±1.71	-0.48±1.33	-0.28±0.33
specimen-C	yes	femur	0.06±0.08	-0.39±0.12	0.22±1.06	-0.41±0.32	0.29±0.38	-0.19±0.12
		tibia	-0.07±0.21	0.08±0.15	-0.19±1.05	0.26±0.27	0.12±0.16	0.05±0.21
	no	femur	-0.45±0.49	0.14±0.29	0.41±3.24	0.01±1.57	-0.63±1.53	0.33±0.51
		tibia	0.25±1.28	0.11±0.51	0.37±3.24	1.22±1.78	0.91±2.99	0.89±0.43

mm respectively. The maximum errors for R_x and R_y were -0.33 ± 0.46 and 0.38 ± 0.47 for the femur and 0.31 ± 0.42 and 0.59 ± 0.77 for the tibia when the filter is used on the fluoroscopy image, while the corresponding values for the case of not employing the filter were 0.38 ± 4.47 and 0.18 ± 4.01 for the femur and 0.35 ± 4.77 and 0.36 ± 4.51 for the tibia. All the translations and rotations are measured in mm and degrees respectively.

In comparison, the precision for out-of-plane translation reported in [13] was 1.22 mm for in-vitro studies of a cadaver knee bone using much higher doses of radiation exposure. The repeatability reported in [12] for T_z was of 3.12 mm, and 2.01 and 2.37 degrees for R_x and R_y respectively. The reported precision in [11] was 8.23 for T_z, 4.13 for R_x and 2.58 for R_y. From these results, it is clear that sub-millimeter and sub-degree accuracy can be achieved using the proposed registration framework for low dose noisy fluoroscopy images of a healthy knee joint. The registration accuracy for the real fluoroscopy data is affected by the accuracy for the distortion correction of the fluoroscopy and errors in the gold standard reference value used to evaluate the exact position of the fluoroscopy and DRR image. The precision of the proposed approach also compares favorably to other similar approaches.

IV. CONCLUSION

In this paper, we have presented an accurate non-invasive approach for in vivo healthy knee joints using a new 3D-2D image registration technique in which a quantum noise and motion blur reduction method is implemented. The experimental results show the accuracy of the proposed registration framework, especially for medial-lateral translation, abduction-adduction rotation and internal-external rotation. In future work we will investigate the use of our approach for tracking the movement of a native knee during regular human activities.

REFERENCES

[1] T. Aach and D. Kunz, "Multiscale linear/median hybrid filters for noise reduction in low dose x-ray images," in *International Conference on Image Processing*, vol. 2. IEEE, 1997, pp. 358–361.

[2] T. Aach, D. Kunz, R. Florent, and S. Makram-Ebeid, "Noise reduction and image enhancement algorithms for low-dose x-ray fluoroscopy." in *Proceedings BVM*, 1996, pp. 95–100.

[3] T. Cerciello, P. Bifulco, M. Cesarelli, L. Paura, M. Romano, G. Pasquariello, and R. Allen, "Noise reduction in fluoroscopic image sequences for joint kinematics analysis," in *XII Mediterranean Conference on Medical and Biological Engineering and Computing 2010*. Springer, 2010, pp. 323–326.

[4] T. Cerciello, M. Romano, P. Bifulco, M. Cesarelli, and R. Allen, "Advanced template matching method for estimation of intervertebral kinematics of lumbar spine," *Medical engineering & physics*, vol. 33, no. 10, pp. 1293–1302, 2011.

[5] G. Gilboa, N. Sochen, and Y. Y. Zeevi, "Variational denoising of partly textured images by spatially varying constraints," *Image Processing, IEEE Transactions on*, vol. 15, no. 8, pp. 2281–2289, 2006.

[6] K. Dabov, A. Foi, V. Katkovnik, and K. Egiazarian, "Image denoising by sparse 3-d transform-domain collaborative filtering," *Image Processing, IEEE Transactions on*, vol. 16, no. 8, pp. 2080–2095, 2007.

[7] M. S. Crouse, R. D. Nowak, and R. G. Baraniuk, "Wavelet-based statistical signal processing using hidden markov models," *Signal Processing, IEEE Transactions on*, vol. 46, no. 4, pp. 886–902, 1998.

[8] M. Elad and M. Aharon, "Image denoising via sparse and redundant representations over learned dictionaries," *Image Processing, IEEE Transactions on*, vol. 15, no. 12, pp. 3736–3745, 2006.

[9] K. Hirakawa and T. W. Parks, "Image denoising using total least squares," *Image Processing, IEEE Transactions on*, vol. 15, no. 9, pp. 2730–2742, 2006.

[10] Y.-L. You and M. Kaveh, "Fourth-order partial differential equations for noise removal," *Image Processing, IEEE Transactions on*, vol. 9, no. 10, pp. 1723–1730, 2000.

[11] Z. Zhu and G. Li, "An automatic 2d–3d image matching method for reproducing spatial knee joint positions using single or dual fluoroscopic images," *Computer methods in biomechanics and biomedical engineering*, vol. 15, no. 11, pp. 1245–1256, 2012.

[12] Z. Zhu, D. F. Massimini, G. Wang, J. J. Warner, and G. Li, "The accuracy and repeatability of an automatic 2d–3d fluoroscopic image-model registration technique for determining shoulder joint kinematics," *Medical engineering & physics*, vol. 34, no. 9, pp. 1303–1309, 2012.

[13] A. A. Muhit, M. R. Pickering, J. M. Scarvell, T. Ward, and P. N. Smith, "Image-assisted non-invasive and dynamic biomechanical analysis of human joints," *Physics in Medicine and Biology*, vol. 58, no. 13, pp. 4679–4702, 2013.

[14] E. Valstar, F. De Jong, H. Vrooman, P. Rozing, and J. Reiber, "Model-based roentgen stereophotogrammetry of orthopaedic implants," *Journal of biomechanics*, vol. 34, no. 6, pp. 715–722, 2001.